Journal of Power Sources 249 (2014) 66–71

Contents lists available at ScienceDirect

Journal of Power Sources

journal homepage: www.elsevier.com/locate/jpowsour

A highly active and long-term stable La-doped $Ba_xSr_{1-x}Co_{1-y}Fe_yO_{3-\delta}$ cathode for solid-oxide fuel cells

Ju-Sik Kim, Dong-Hee Yeon*, Doh Won Jung, Chan Kwak

Samsung Advanced Institute of Technology (SAIT), 14-1 Nongseo-dong, Yongin-si 446-712, Republic of Korea

HIGHLIGHTS

- DFT calculations reveal BLSCF cathode has more phase stability than BSCF cathode.
- La addition in BSCF cathode reduces lattice distortions and the cation clustering.
- The impedance of BLSCF was 0.04 Ω cm^2 at 973 K and maintained over 800 h.
- A large tubular cell with a BLSCF cathode exhibited power density of 0.52 W cm^{-2}.
- In a tubular cell, the electrochemical activity is maintained over 950 h.

ARTICLE INFO

Article history:
Received 14 August 2013
Received in revised form
2 October 2013
Accepted 14 October 2013
Available online 21 October 2013

Keywords:
Solid oxide fuel cells
Cathode
Perovskite
BSCF
Phase stability

ABSTRACT

$Ba_{0.5}Sr_{0.5}Co_{0.8}Fe_{0.2}O_3$ (BSCF)-based perovskite oxides have attracted much attention as cathode materials with novel catalytic properties in intermediate-temperature solid-oxide fuel cells (IT-SOFCs). The phase stability of these materials, however, is one of the huge obstacles for the commercialization of IT-SOFCs. Here, we examine the long-term stability and the electrochemical properties of La-doped BSCF (BLSCF) in which Ba was partially substituted with La to enhance the phase stability without losing the catalytic activity. From symmetric cell measurements, the initial electrode impedance of BLSCF was found to be 0.04 Ω cm^2 in air at 973 K; it remained nearly constant even after 800 h, in contrast to BSCF without La doping. It was further demonstrated that a large tubular cell consisting of a BLSCF cathode exhibited a high maximum power density of 0.52 W cm^{-2} and impressive long-term stability at 973 K. Free-energy calculations using density functional theory and XRD experiments for these cathodes showed that the addition of La into BSCF cathode makes the cubic structure of the cathode stable and the phase transition into the hexagonal phase is prohibited. The excellent electrochemical activity of BSCF based cathode is maintained over 950 h in a large tubular cell.

1. Introduction

Solid-oxide fuel cells (SOFCs), which are highly efficient, fuel-flexible energy conversion devices, have received a considerable amount of attention due to dwindling fossil fuel reserves. In recent years, many studies focusing on the commercialization of SOFCs have attempted to operate SOFCs in the intermediate temperature range (700 °C or lower) for the purpose of enhancing the long-term stability and reducing costs [1–5]. One of the main hurdles in the development of intermediate-temperature SOFCs (IT-SOFCs) with a thin electrolyte is the large impedance for the oxygen reduction reaction at the cathode [1,3,6]. The problem of large cathodic impedance can be solved by the introduction of mixed-conducting perovskite oxides with high catalytic ability, in which ions and electrons can be conducted simultaneously to extend the electrochemical active sites [3,5,6].

Among mixed-conducting oxides, $Ba_{0.5}Sr_{0.5}Co_{0.8}Fe_{0.2}O_3$ (BSCF) has received significant attention regarding its application as a promising cathode material for low-temperature SOFCs due to its remarkable electrochemical properties [3,7–9]. BSCF has an ABO_3 type cubic perovskite structure, where A-site cations consist of Ba and Sr, and B-site cations consist of Co and Fe, respectively. The structural stability of BSCF still limits its practical use as a BSCF cathode for IT-SOFC. Below 900 °C, BSCF undergoes a phase transition from a cubic to a hexagonal structure which has lower catalytic activity as compared to the cubic phase. Therefore, the performance of BSCF-based cathode is degraded with time due to the formation of the hexagonal phase, when operated at a temperature below 900 °C [10–12].

According to the literature dealing with the structural changes of BSCF [13–16], the phase transition is affected by the lattice

* Corresponding author. Tel.: +82 31 280 8469; fax: +82 31 280 6739.
E-mail address: donghee.yeon@samsung.com (D.-H. Yeon).

0378-7753/$ – see front matter © 2013 Elsevier B.V. All rights reserved.
http://dx.doi.org/10.1016/j.jpowsour.2013.10.053

distortion which is known to be attributable to the valence changes of B-site cations [10,13,14]. Especially, Co likely brings about the severe lattice distortion of BSCF, due to its short bond-length with oxygen and low spin configuration [10,13,17]. Although reducing Co contents enhance the stability of cubic phase, however, a high content of Co above 0.6 is still required for low cathodic polarization resistance [18]. When the content of Co decreased from 0.8 to 0.6, the lattice parameter, oxygen nonstoichiometry and free energy were not highly changed in the literature [13,18], and thus the long-term stability of cubic phase would not be significantly improved by the small change of Co content.

The phase transition of BSCF is also dependent on the doping contents of the A-site cations, as the structural change occurs via the partial decomposition into Ba-rich and Sr-rich phases. In BSCF cathode, Ba plays an important role in preventing the formation of the vacancy-ordered brownmillerite phase [17,19]. Increasing Ba content, however, results in clustering of A-site cations due to the small ionic size and the preferential interactions between Ba and Ba ions. Considering the Goldschmidt tolerance factor regarding the lattice distortion [11,14], the partial substitution of Ba with a large metal ion such as La is expected to cause the stabilization of the cubic phase by suppressing the structural changes, especially at low operating temperature ranges below 900 °C. Some attempts have been made to add the La into BSCF to enhance the cathodic performance [20,21]. These works, however, conducted mainly the electrochemical kinetics and were not focused on the phase stability when La is doped to BSCF.

The goal of the present study was theoretically to examine the effect of La doping on the phase transition of BSCF and experimentally to verify the long-term stability of a La-doped BSCF cathode at an operation temperature of 700 °C.

2. Experiment and simulation

2.1. Experimental syntheses and characterizations of $Ba_{0.5}Sr_{0.5}Co_{0.8}Fe_{0.2}O_3$ (BSCF) and $Ba_{0.2}La_{0.3}Sr_{0.5}Co_{0.6}Fe_{0.4}O_3$ (BLSCF) powders

BSCF and BLSCF powders were synthesized using the Pechini method. In BLSCF, only Ba was partially substituted with La, while Sr kept a constant stoichiometry of 0.5 for high catalytic activity, because a high content of Sr is required for a high concentration of oxygen vacancies [22,23]. An aqueous solution for the Pechini method was prepared by adding $Ba(NO_3)_2$ (Sigma Aldrich, 99.9%), $La(NO_3)_3 \cdot 6H_2O$ (Alfa Aesar, ACS 99.9%), $Sr(NO_3)_2$ (Alfa Aesar, ACS 99.0%), $Co(NO_3)_2 \cdot 9H_2O$ (Alfa Aesar, ACS 99.9%), and $Fe(NO_3)_3 \cdot 9H_2O$ (Junsei, ACS 99.9%) to distilled water in the correct molar ratios, then mixing this with citric acid (99.5%, Aldrich) to produce a solution with a citric acid/metal-ion ratio of 1:1. The solution was evaporated at 573 K and the resulting powders were calcinated at 1273 K for 4 h.

The powders were then ground with zirconia balls in ethyl alcohol for 24 h using a planetary mill in order to break up agglomerates and form nanoparticles.

To identify the crystal structures of the powders, the resulting powders heated at various temperatures (700–800 °C) after the final calcination step were characterized using an X-ray diffractometer (XRD, X'pert, Philips). The scanning speed was 4° per minute and the step size was 0.03°.

2.2. Simulation procedure

The first-principle calculations were performed by means of density functional theory (DFT) with a plane-wave basis set and ultra-soft pseudopotentials. The Perdew–Burke–Ernzehof (PBE) type of exchange-correlation GGA functional was used. We employed the Vienna ab initio Simulation Package (VASP) [24]. For the perovskite-type crystal structure of BSCF, we used $2 \times 2 \times 2$ supercells containing 4 Ba atoms, 4 Sr atoms, 6 Co atoms and 2 Fe atoms with 24 oxygen atoms, which correspond to the $Ba_{0.5}Sr_{0.5}Co_{0.75}Fe_{0.25}O_3$ formula unit. For BLSCF cathode, 2 Ba atoms of BSCF supercell were substituted with La atoms, which correspond to the $Ba_{0.25}$ $La_{0.25}Sr_{0.5}Co_{0.75}Fe_{0.25}O_3$ formula unit. The ratio between Co and Fe atoms was not changed to clarify the effect of La atoms. The stoichiometry of the BSCF and BLSCF cathodes used in simulations was slightly different with those in experiments due to the limited numbers of atoms permitted in DFT calculations. The kinetic energy cut-off of the plane-wave basis was set to 600 eV and the $4 \times 4 \times 4$ k-point mesh was created by the Monkhorst-pack scheme. Spin-polarized calculations were performed for the different atomic arrangements in the supercells. The lattice parameters and the atomic positions of the supercells for the given atomic arrangement were determined by DFT calculations.

2.3. Electrochemical measurements

Electrode performance levels were measured using symmetric cells as follows; cathode-GDC(buffer layer)-ScSZ(electrolyte)-GDC(buffer layer)-cathode. These symmetric configurations can be found commonly in pervious researches [19,23]. To fabricate the symmetric cell, ScSZ ($Zr_{0.8}Sc_{0.2}O_2$, FCM) powders were pressed into a pellet and then sintered at 1450 °C for 5 h in air. In each cell, the dense electrolyte pellet was ~1.2 mm thick and 0.5 cm in diameter. GDC ($Ce_{0.9}Gd_{0.1}O_2$, BET: 11.8 $m^2\ g^{-1}$, FCM, USA) paste was then screen-printed as the buffer layer on both surfaces of the zirconia electrolyte, followed by heating to 1200 °C for 2 h in air. The cathode paste, which prepared using a three-roll mill, was subsequently coated onto the buffer layer surface using a screen-printing method and then fired at 900 °C for 2 h in air. The cathode active area was 0.785 cm^2. Ag paste (H4580, Shoei Chemical, Japan) and Ag wire were used to form the electrical connections to both electrodes.

The impedance spectra were measured at an open circuit in galvanostatic mode over a frequency range of 0.1 Hz–10 kHz using 10 mV of AC perturbation with a potentiostat (Gamry Instruments, USA). For the impedance measurements, the margin of error in the reported polarization resistances is estimated to be less than 5% based on measurements from three cells for each type of cathode material (BSCF and BLSCF).

For the full cell test, an anode-supported tubular cell (diameter: 2.2 cm, thickness: 0.2 cm) with a large cathode area (34.5 cm^2) was prepared. The cell configuration of the tubular cell was cathode|GDC (buffer layer)|ScSZ (solid electrolyte)|AFL| NiO–YSZ, where AFL denotes the anode functional layer and YSZ denotes yttria-stabilized zirconia. For the construction of the tubular cell, a commercial anode support (Khancera, Korea) composed of NiO and YSZ was used. AFL slurry with submicron-sized NiO (Sumitomo, Japan) and nano-sized ScSZ (FCM, USA) was first coated onto the surface of the anode support using a dip-coating technique and was then heated to 900 °C for 2 h. The electrolyte slurry containing ScSZ was coated on top of the AFL layer in the same manner, which was followed by co-firing at 1350 °C for 5 h. The GDC slurry as a buffer layer was coated onto the electrolyte and fired at 1200 °C for 2 h, after which the cathode slurry was finally dip-coated and then fired at 900 °C for 2 h.

The current–voltage characteristics were evaluated and a galvanostatic duration test of the tubular cell was carried out as a function of time at 700 °C using an electronic loader (Wonatech, Korea). For the fuel cell test, the fuel sent to the anode was humidified (3% H_2O) H_2 with a constant flow rate of 120 ml min^{-1}.

In order to avoid a detrimental reaction of the cathode material with CO_2 or H_2O, the cathode was exposed to dry air (CO_2:0.033 vol %, H_2O <0.1 vol%) during the long-term operation.

3. Results and discussion

Firstly, in order to investigate the effect of the La content on the phase transition of BSCF, first-principle supercell calculations of BSCF and La-doped BSCF (BLSCF) perovskites were performed. Many DFT calculation studies for the BSCF perovskite were performed for its defect structure, material properties and diffusion mechanism [13,15,25–29]. Configurations of 2 × 2 × 2 supercells for cubic and hexagonal structures were employed for the calculations. The energies of the supercells for the cubic phase and the hexagonal phase of BSCF are −261.005 eV and −266.403 eV, respectively. The calculated energies for the BLSCF phases are −274.269 eV and −276.551 eV for the cubic and hexagonal phases, respectively. The energy differences between the cubic and hexagonal phases are 5.398 eV and 2.282 eV for the BSCF and BLSCF, respectively, which can be regarded as the driving force for the phase transition.

The small driving force for the hexagonal phase transition of BLSCF is due to the addition of La to BSCF, which enhances the stability of the cubic structure. The free energies of the cubic structures are highly dependent on the lattice distortion, which results in a change in the inter-atomic distances between cobalt and oxygen atoms. Indeed, the maximum and minimum inter-atomic distances between Co and oxygen for cubic BSCF were determined to be 2.349 Å and 1.811 Å, respectively, which deviated by +19.5% and −7.8% from the ideal inter-atomic distance of 1.965 Å. On the other hand, deviations of approximately ±1.5% in the inter-atomic distance were evaluated in the BLSCF case. Thus, it is reasonable to conclude that the addition of La to BSCF suppresses the Jahn–Teller distortion caused by the variation in the atomic distance, leading to the stabilization of the cubic phase.

In order to estimate the phase transition temperature, the entropic contributions to the free energies were obtained by phonon-mode calculations using the PHONOPY code [30]. The free energy differences between the cubic and hexagonal phases are shown in Fig. 1 for BSCF and BLSCF systems, respectively. From Fig. 1, it is recognized that the transition temperature of BLSCF is lower than that of BSCF due to the enhancement of the stability of the cubic phase caused by the suppression of the lattice distortion. To provide additional insight into the phase stabilization process upon the addition of La, we calculated the free energies of BSCF and BLSCF for various atomic arrangements in supercell structures, as shown in Fig. 2. From the first-principles calculations, these energies were found to be highly dependent on the arrangement of the A-site atoms, whereas the energy differences in the arrangements of different B-site atoms are negligible. Here, the A-site coordination number (CN) for Sr–Sr atoms is defined as the average number of Sr among the nearest A-site atoms with one Sr atom. A-site CN for Sr–Sr atoms has values of 0, 3, and 6 for fully ordered, randomly distributed and fully clustered atomic arrangements, respectively. In Fig. 2, it should be noted that the free energy of BSCF decreased with an increase in the CN value, while BLSCF had the lowest level of free energy at a CN value of 2. These results indicate that Sr in BSCF prefers to be surrounded by the same atoms, whereas Sr in BLSCF tends to be partially separated. Based on these results regarding the free energy changes shown in Figs. 1 and 2, it is suggested that the addition of La plays an important role in inhibiting the lattice distortion and the phase formations of local $BaCoO_3$ or $SrCoO_3$.

To substantiate the validity of the theoretical results based upon a first-principles calculation, we experimentally investigated the

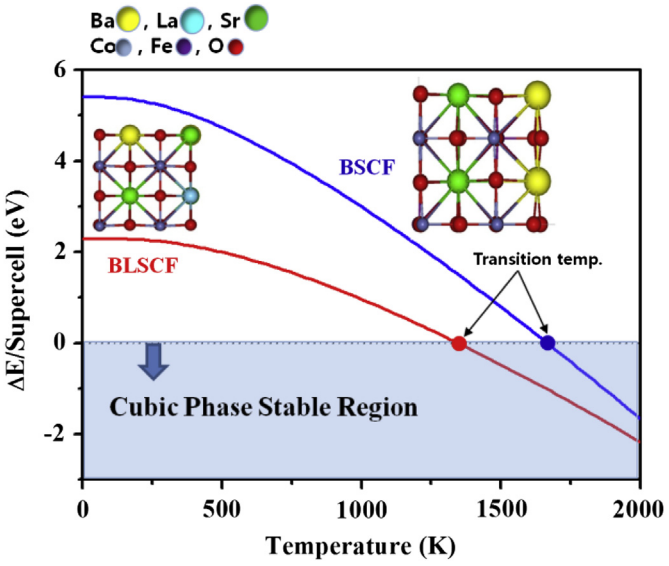

Fig. 1. Free energy differences between cubic and hexagonal structures of BSCF and BLSCF as a function of temperature. Stable cubic structures corresponding to those oxides were displayed as well, which shows that BSCF structure is more distorted in comparison with BLSCF structure.

structures of BSCF and BLSCF phases for different heating temperatures. The XRD patterns of BSCF and BLSCF bulk powders are illustrated in Fig. 3(A) and (B), respectively. The well-known cubic perovskite structure was detected in both samples when they were heated to 1000 °C for 100 h in air. When the BSCF pellet was aged at 800 and 700 °C for 100 h, however, a hexagonal phase marked with a closed triangle was observed at 27 and 43°. As the heating

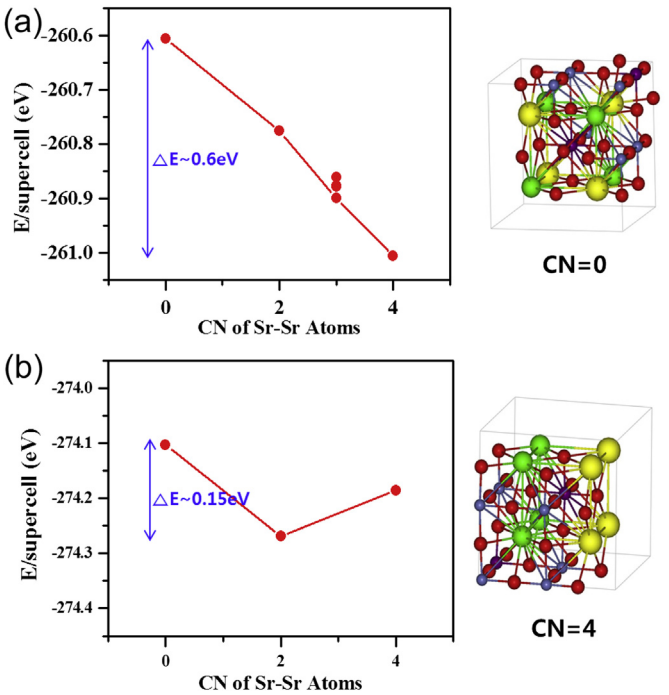

Fig. 2. Free energies for cubic structures of (a) BSCF and (b) BLSCF as a function of A-site coordination number (A-site CN) for Sr–Sr atoms. BSCF has lower free energy as the coordination number for Sr–Sr atoms increases. The free energy of BLSCF has a lowest value at A-site CN = 2, which represent that BLSCF prefer the randomly distributed cation configuration.

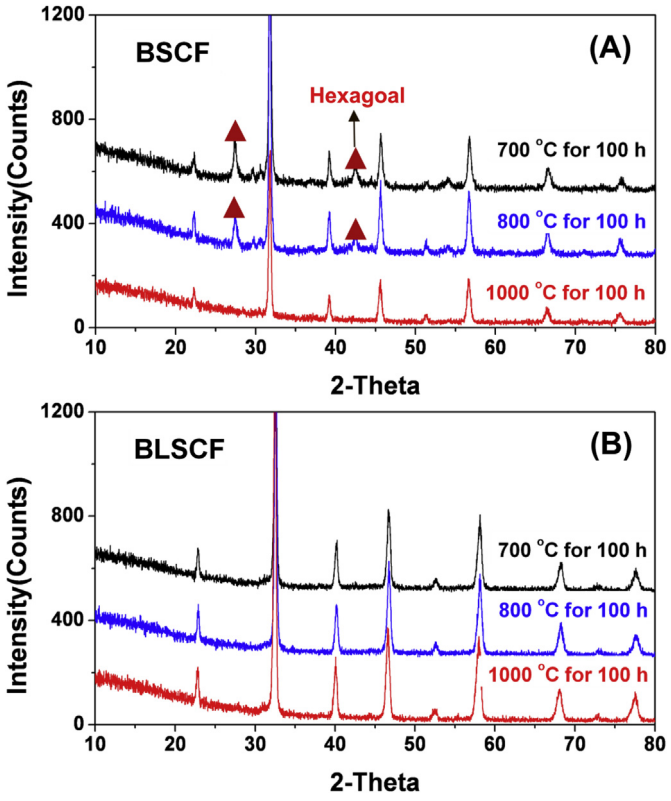

Fig. 3. XRD patterns of (A) BSCF and (B) BLSCF bulk powders heated to various temperatures for 100 h after initial calcination in air at 1000 °C.

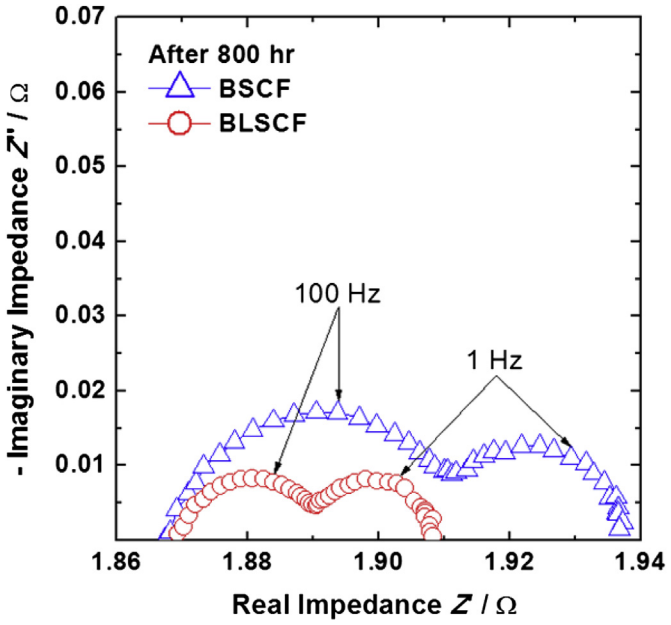

Fig. 4. Nyquist plots of AC-impedance data obtained from symmetric cells with BSCF and BLSCF. The data was collected at 700 °C in air.

temperature decreased, the intensity of the diffraction peaks for the hexagonal phase showed a corresponding increase. It is noteworthy that the hexagonal phase was not found in the XRD pattern of the BLSCF pellet, even after heating it to 700 and 800 °C. Thus, the BLSCF is expected to have a stable cubic phase at an operating temperature of 700 °C. This result confirms that La doping suppresses the formation of the hexagonal phase, as suggested in the theoretical analyses based on the free energy for the perovskite structure.

In order to assess the effect of a phase change on the electrode performance, the AC impedances of symmetric cells were measured over time at 700 °C in air for BSCF and BLSCF electrodes. The ohmic losses were consistent with the electrolyte thickness and did not change with time. The polarization impedances R_p for the as-prepared BSCF and BLSCF electrodes had comparable values of 0.037 and 0.04 Ω cm^2, respectively. This low impedance of the BLSCF electrode demonstrates that the doping of La has no significant detrimental effects on the cathodic performance because it enhances the electrical conductivity [20,21].

After 800 h passed, however, the R_p value for the BSCF rose to 0.069 Ω cm^2, while the electrode impedance of BLSCF showed the nearly the same value of 0.04 Ω cm^2 regardless of the time, as shown in the Nyquist plots of the impedance spectra in Fig. 4. In particular, the high frequency arc for the BSCF electrode was significantly larger in magnitude than this arc for the BLSCF electrode, which is associated with the surface exchange reaction as affected by the catalytic properties of cathode materials [31]. The increased impedance for the BSCF could be attributed to the clustering of particles. From the image analysis of SEM, however, the mean particle size was found to have an almost constant value of about 0.45 μm even after 800 h. The hexagonal phase of BSCF has poor catalytic activity for oxygen reduction as compared to the cubic phase due to its low diffusivity of oxygen vacancies. Keeping in mind that the cubic phase of BSCF partially changes at 700 °C to the hexagonal phase over time, the increase in the electrode impedance after 800 h may be due to the phase transition to the hexagonal phase. Consequently, this implies that the unchanged impedance of the BLSCF electrode is attributed to the stabilization of the cubic phase as induced by the addition of La.

We also examined the long-term performance of an anode-supported tubular fuel cell in which BLSCF were used as the cathode. A scanning electron microscopy (SEM) image of this tubular cell is shown in Fig. 5. The SEM images indicate that the BLSCF forms a uniform coating over the surfaces of the GDC without interfacial reaction layers by solid-state reaction. Fig. 6(A) plots the voltage–current polarization curve for this fuel cell at 700 °C and shows a high maximum power density of 0.52 W cm^{-2} using an YSZ-based electrolyte. Fig. 6(B) displays the operating power as a function of time when the cell was subjected to a constant current of 7.6 A. It is remarkable that the performance remained essentially unchanged for the 950 h duration of the experiment. This result is consistent with impedance results obtained for the symmetric cells. Taken together, the free energy calculations, the impedance and *V–I* curve duration data demonstrate that the doping of La into BSCF effectively prevents a phase transition, which high performance and long-term stability are realized for a fuel cell with BLSCF as the cathode. This result strongly implies that the commercial application of BSCF-based materials with novel catalytic properties for SOFCs or solid-oxide electrolysis (SOE) electrodes possibly is attainable with an addition of La to BSCF cathode.

4. Conclusions

In conclusion, the results obtained in this study theoretically and experimentally demonstrated that the partial substitution of Ba with La caused a significant increase in the long-term stability without the catalytic loss for oxygen reduction. The addition of La plays an important role in preventing the formation of hexagonal phase caused by cation clustering, leading to the markedly higher stability of BLSCF compared to BSCF.

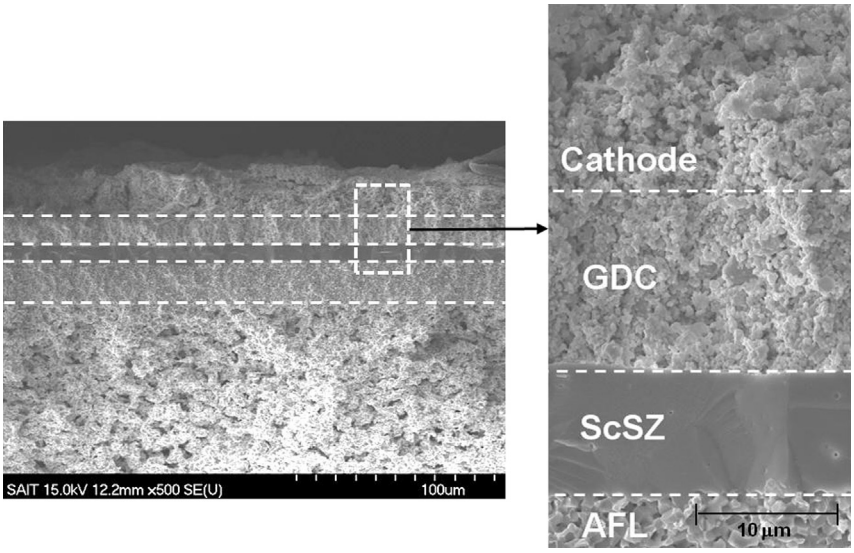

Fig. 5. Cross-sectional SEM images of the anode-supported tubular cell.

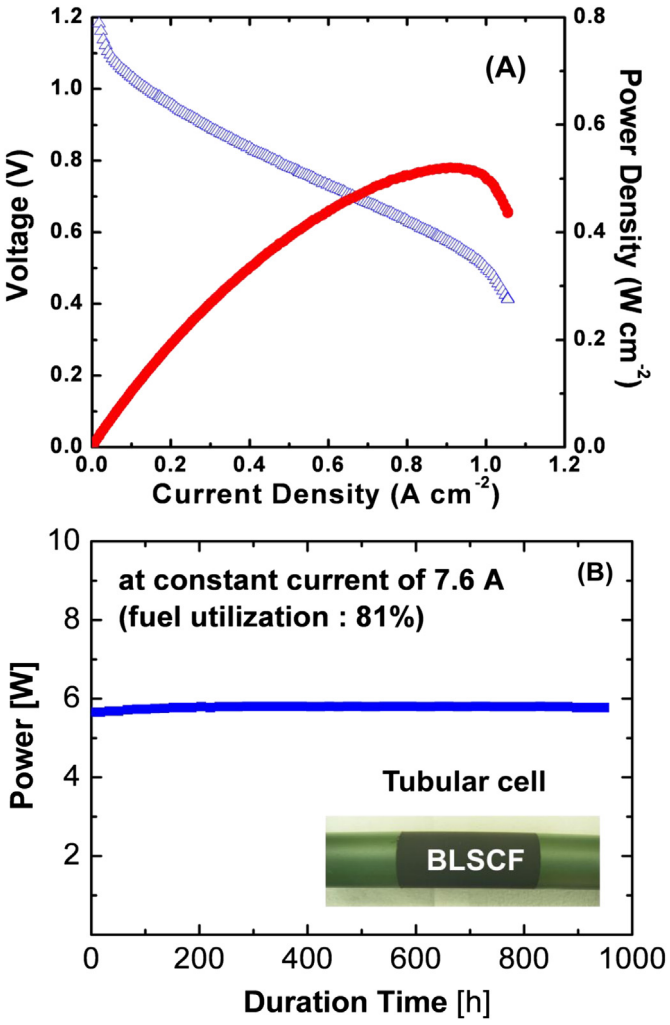

Fig. 6. (A) *V–I* polarization curves at 700 °C for anode-supported fuel cells with a BLSCF cathode and a Ni–ScSZ anode, and (B) power corresponding to the fuel cell at a constant current of 7.6 A as a function of time.

Acknowledgments

We would like to thank Dr. Han Wool Yu and Dr. Eun Soo Lee for supplying the tubular-cell test equipment.

References

[1] N.P. Brandon, S. Skinner, B.C.H. Steele, Annu. Rev. Mater. Res. 33 (2003) 183–213.
[2] S.C. Singhal, K. Kendall, High Temperature Solid Oxide Fuel Cells: Fundamentals, Design, and Applications, Elsevier Advanced Technology, UK, 2003.
[3] Z. Shao, S.M. Halle, Nature 431 (2004) 170–173.
[4] Y. Masaya, T. Atsuko, S. Mitsuru, H. Takashi, Solid State Ionics 177 (2007) 3351–3359.
[5] W. Zhou, R. Ran, Z. Shao, J. Power Sources 192 (2009) 231–246.
[6] J.M. Vohs, R.J. Gorte, Adv. Mater. 21 (2009) 943–956.
[7] Q.L. Liu, K.A. Khor, S.H. Chan, J. Power Sources 161 (2006) 123–128.
[8] S. Li, Z. Lü, N. Ai, K. Chen, W. Su, J. Power Sources 165 (2007) 97–101.
[9] Y.H. Lim, J. Lee, J.S. Yoon, C.E. Kim, H.J. Hwang, J. Power Sources 171 (2007) 79–85.
[10] M. Arnold, T.M. Gesing, J. Martynczuk, A. Feldhoff, Chem. Mater. 20 (2008) 5851–5858.
[11] D.N. Mueller, R.A. De Souza, T.E. Weirich, D. Roehrens, J. Mayer, M. Martin, Phys. Chem. Chem. Phys. 12 (2010) 10320–10328.
[12] E.G. Babakhani, J. Towfighi, L. Shirazi, A.N. Pour, J. Membr. Sci. 376 (2011) 78–82.
[13] M. Yoshiya, C.A.J. Fisher, Y. Iwamoto, M. Asanuma, J. Ishii, K. Yabuta, Solid State Ionics 172 (2004) 159–163.
[14] S. Švarcová, K. Wiik, J. Tolchard, H.J.M. Bouwmeester, T. Grande, Solid State Ionics 178 (2008) 1787–1791.
[15] E.A. Kotomin, Y.A. Mastrikov, M.M. Kuklja, R. Merkle, A. Roytburd, J. Maier, Solid State Ionics 188 (2011) 1–5.
[16] M.M. Kuklja, Y.A. Mastrikov, B. Jansang, E.A. Kotomin, Solid State Ionics 230 (2013) 21–26.
[17] S. McIntosh, J.F. Vente, W.G. Haije, D.H.A. Blank, H.J.M. Bouwmeester, Chem. Mater. 18 (2006) 2187–2193.
[18] Z. Chen, R. Ran, W. Zhou, Z. Shao, S. Liu, Electrochim. Acta 52 (2007) 7343–7351.
[19] Z. Shao, G. Xiong, J. Tong, H. Dong, W. Yang, Sep. Purif. Technol. 25 (2001) 419–429.
[20] D. Beckel, U.P. Muecke, T. Gyger, G. Florey, A. Infortuna, L.J. Gauckler, Solid State Ionics 178 (2007) 407–415.
[21] X. Ding, X. Kong, J. Jiang, C. Cui, X. Guo, Mater. Res. Bull. 45 (2010) 1271–1277.
[22] H. Kruidhof, H.J.M. Bouwmeester, R.H.E. Van Doorn, A.J. Burggraaf, Solid State Ionics 63–65 (1993) 816–822.
[23] L. Qiu, T.H. Lee, L.M. Liu, Y.L. Yang, A.J. Jacobson, Solid State Ionics 76 (1995) 321–329.
[24] G. Kresse, J. Furthmueller, VASP the Guide, Univ. Vienna, Vienna, Austria, 2003.
[25] S. Ganaopadhayay, T. Inerbaev, A.E. Masunov, D. Altilio, N. Orlovskaya, Appl. Mater. Interfaces 1 (2009) 1512–1519.

[26] S. Ganaopadhayay, A.E. Masunov, T. Inerbaev, J. Mesit, R.K. Guha, A.K. Sleiti, J.S. Kapat, Solid State Ionics 181 (2010) 1067–1073.
[27] M.M. Kuklja, Y.A. Mastrikov, S.N. Rashkeev, E.A. Kotomin, ECS Trans. 35 (2011) 2077–2084.
[28] C. Wessel, M.-W. Lumey, R. Dronskowski, J. Membr. Sci. 366 (2011) 92–96.
[29] M.M. Kuklja, Y.A. Mastrikov, N. Janjang, E.A. Kotomin, J. Phys. Chem. C 116 (2012) 18605–18611.
[30] A. Togo, F. Oba, I. Tanaka, Phys. Rev. B 78 (2008) 134106–134114.
[31] F.S. Baumann, J. Fleig, H.U. Habermeier, J. Maier, Solid State Ionics 177 (2006) 3187–3191.